The spatial extent of rainfall events and its relation to precipitation scaling

Lochbihler, Kai; Lenderink, Geert; Siebesma, A. Pier

DOI
10.1002/2017GL074857

Publication date
2017

Document Version
Final published version

Published in
Geophysical Research Letters

AGU PUBLICATIONS

Geophysical Research Letters

RESEARCH LETTER
10.1002/2017GL074857

Key Points:
- Peak intensity of rainfall events increases with spatial extent of the rain cells
- Only large-area rainfall events display super Clausius-Clapeyron scaling of peak intensities
- Event size has to increase beyond a critical value of dew point temperature in order to support super CC scaling

Supporting Information:
- Supporting Information S1

Correspondence to:
K. Lochbihler,
kai.lochbihler@knmi.nl

Citation:
Lochbihler, K., G. Lenderink, and A. P. Siebesma (2017), The spatial extent of rainfall events and its relation to precipitation scaling, *Geophys. Res. Lett.*, *44*, 8629–8636, doi:10.1002/2017GL074857.

Received 7 JUL 2017
Accepted 8 AUG 2017
Accepted article online 14 AUG 2017
Published online 26 AUG 2017

The spatial extent of rainfall events and its relation to precipitation scaling

Kai Lochbihler[1,2], Geert Lenderink[1], and A. Pier Siebesma[1,2]

[1]The Royal Netherlands Meteorological Institute (KNMI), De Bilt, Netherlands, [2]Department of Geoscience and Remote Sensing, Faculty of Civil Engineering and Geosciences, Delft University of Technology, Delft, Netherlands

Abstract Observations show that subdaily precipitation extremes increase with dew point temperature at a rate exceeding the Clausius-Clapeyron (CC) relation. The understanding of this so-called super CC scaling is still incomplete, and observations of convective cell properties could provide important information. Here the size and intensity of rain cells are investigated by using a tracking of rainfall events in high-resolution radar data. Higher intensities are accompanied by larger rainfall areas. However, whereas small rain cells mainly follow CC scaling, larger cells display super CC behavior. Even more, for dew point exceeding 15°C, the rain cell size has to increase in order to sustain super CC scaling and a remarked increase in rain cell area is found. Our results imply that the source area of moisture, the cloud size, and the degree of mesoscale organization play key roles in the context of a warming climate.

1. Introduction

A warmer atmosphere can hold more water. As a consequence rainfall amounts increase and precipitation extremes intensify. This relation is generally referred to as precipitation scaling. More precisely, the scaling rate is the fractional rate of change of rainfall with respect to temperature or moisture availability. Global climate models, for instance, predict that extremes of daily precipitation sums, on average, increase up to 6–7% per degree warming [*Allen and Ingram*, 2002; *Tebaldi et al.*, 2006; *Pall et al.*, 2007; *Kharin et al.*, 2013]. This is in line with the Clausius-Clapeyron (CC) equation, which describes the water holding capacity of the atmosphere with respect to temperature [*Trenberth et al.*, 2003]. However, focusing on much smaller-scale convective extremes, it has become evident that on subdaily and, in particular, subhourly time scales scaling rates can exceed the CC relation (called super CC scaling) even by up to the factor of 2 (called 2CC scaling) [*Lenderink and van Meijgaard*, 2008; *Loriaux et al.*, 2013; *Mishra et al.*, 2012; *Lenderink et al.*, 2011]. These results have been obtained by deriving the dependency of high percentiles (usually the 99th) of the rainfall distribution on surface temperature or dew point temperature from present-day short-term variability. This is usually done by a binning approach, in which precipitation intensities are paired to coincident near-surface (dew point) temperatures [*Westra et al.*, 2014].

The cause of super CC scaling of convective precipitation extremes on short time scales is still subject of ongoing research. Statistical effects related to the duration and type of precipitation events complicate the computation of scaling rates and their physical interpretation [*Haerter and Berg*, 2009; *Molnar et al.*, 2015; *Wasko et al.*, 2015; *Wasko and Sharma*, 2015]. Besides these statistical effects, dynamical effects are generally considered to play an important role [*Westra et al.*, 2014; *Trenberth et al.*, 2003]. According to this hypothesis, the release of latent heat due to condensation in a cloud updraft increases buoyancy and leads to stronger cloud dynamics [*Loriaux et al.*, 2013]. This in turn causes enhanced moisture convergence, possibly from a larger area. This positive feedback may lead to a 2CC behavior [*Loriaux et al.*, 2013; *Lenderink et al.*, 2017]. Recent results with a convection- intensities but smaller spatial extent [*Wasko et al.*, 2016].

The listed aspects bring out the multidimensionality of the scaling relationship between precipitation extremes and surface temperature and moisture. In situ observations contributed substantially to the detection and exploration of super CC scaling. However, to further expand our knowledge about convective precipitation extremes in this context, we need to look at finer details such as the area and intensity of individual showers. Rain radar data provide a high spatial and temporal resolution. At the same time, following precipitation events through time and space creates a perspective that makes it possible to investigate their characteristics throughout the whole life cycle [*Moseley et al.*, 2013] and allows an easier interpretation in

terms of physical processes. Here we exploit the potential of a high-resolution rain radar data set using rain cell tracking and investigate the spatial properties and intensity of precipitation events and its relation to surface moisture. Therefore, we use dew point temperature T_d because it is a direct measure of humidity and gives more robust scaling results than temperature [*Lenderink et al.*, 2011; *Lenderink and van Meijgaard*, 2010]. More specifically, we focus on the following two questions: (1) what is the relation between rainfall area/level of organization and precipitation intensity and (2) how do these factors change with the surface dew point temperature.

2. Data and Methods

We make use of two data sets provided by the Royal Netherlands Meteorological Institute (KNMI). First, a time series of radar-based precipitation fields spanning the years from 2008 to 2016 with a time step of 5 min and a spatial resolution of 1 km [*Overeem et al.*, 2009a, 2009b]. For this study we select a region within a buffer of approximately 10 km around the land surface of the Netherlands (see Figure S1). The domain covers an area of 57,000 km^2 (roughly 280 km by 200 km). Second, we use T_d records from in situ data of the KNMI automatic weather stations (AWSs) network. For the same period as the radar data hourly time series from 35 AWSs are available (see Figure S1 in the supporting information). The majority of stations are free from missing values. To study the characteristics of summertime convective precipitation, we only select the months from April to September.

Using the conceptual framework of *Moseley et al.* [2013], we developed an algorithm to track precipitation events in rain radar data. Figure 1 shows a simplified illustration of how a track or event—we use these terms as synonyms—is defined. In the first step a clustering routine detects rain cells in each time step, defined as a continuous area of grid points exceeding an intensity threshold of 0.6 mm/h. At this point we determine the rain cell properties such as area, maximum intensity, and the location of the intensity weighted center of mass which is used for all distance calculations. Then a linking procedure checks for (partly) overlapping cells in subsequent time steps. The results are used to estimate how fast rain cells move between time steps. The velocities of cells that do not split or merge are averaged over a grid of 150 km by 180 km (see Figure S1) and are used as an approximation of the large-scale cloud advection velocity. An iterative procedure takes this velocity to advect the rain cells, rechecks for new overlaps, and updates the velocity fields. After six iterations the procedure converges, and the final links between rain cells are established to derive the rain cell tracks. There are two types of tracks: without and with splitting and/or merging of rain cells. To see an example of the first possibility, the so-called solitary track, we have to ignore the green haloed cells in Figure 1. If all cells were present, we would have a more complex version which involves splitting and merging of rain cells. We consider both track types in this paper equally, unless denoted otherwise. Furthermore, we define the peak of an event as the cell with the highest maximum intensity (yellow frame in Figure 1). The size of a cell is represented by the square root of its area ($\sqrt{A}$).

To be taken into account for further analysis, tracks must initiate and end in the selected radar data region without crossing the boundaries. Two additional filters are applied. First, all tracks of shorter duration than three time steps (15 min) are omitted to limit the analysis to events with a complete life cycle (start, peak, and decay). Second, the distance between the first and last cell of a track must be at least 5 km. This removes stationary tracks which are most likely the result of pseudorain caused by ground echoes (compare Figures S2 and S3). Events which pass these filters are connected to a T_d record measured at the closest station (with data available) 3 h ($\pm$30 min) before and at the location of the peak of the event.

To relate dew point temperature with precipitation event area and intensity, we make use of binning methods with either constant bin widths or bin sizes. In the first case we divide the T_d range into discrete equally spaced intervals. For the latter, the bin breaks are chosen to achieve approximately equal numbers of events within each bin. This procedure leads to varying bin widths, but, in contrast to a constant bin width, it allows us to include events which occur at very high T_d.

3. Results

3.1. Rain Cell Tracking and Cell Characteristics

The rain cell tracking reveals a total number of approximately 1.52×10^5 tracks (with $T_d > 5$°C). Of these, 99% can be connected with a T_d record from an AWS within a range of less than 35 km. The average distance is 16.4 km. Most of the events (62%) are solitary tracks. However, the percentage of solitary tracks steadily

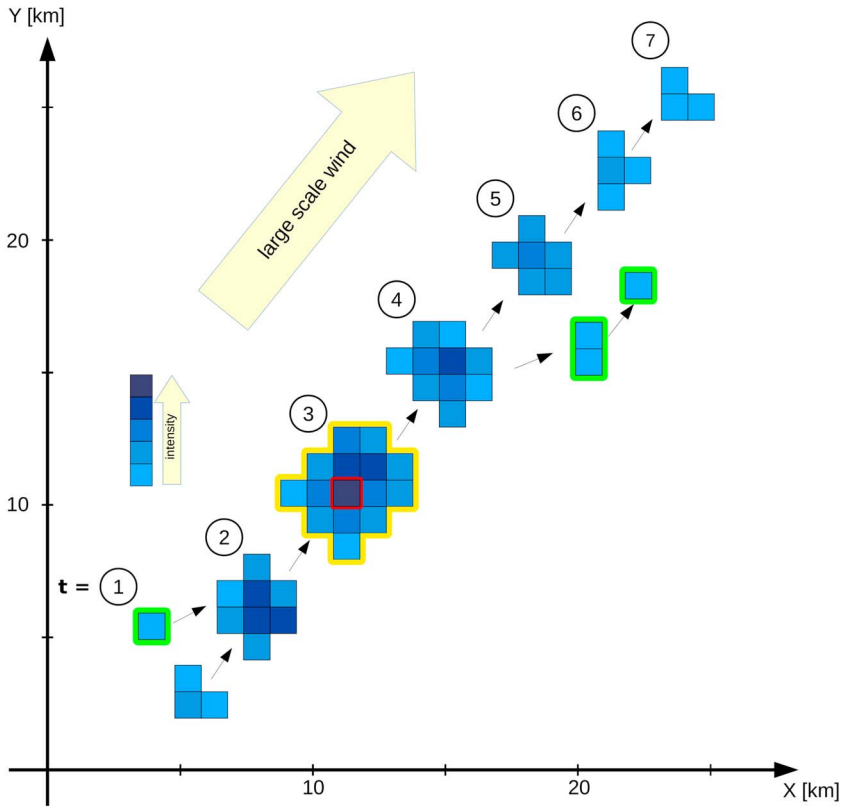

Figure 1. Idealized version of a rain cell track showing how rain cells are advected with the large-scale wind during the life cycle ($t = 1, 2, \ldots, 7$). Splitting and/or merging of rain cells can happen at any time. Without those cells (green halo) our example would be a so-called solitary track. The yellow framed cell holds the maximum intensity (red grid point). Note that this is a composite showing all rain cells (time steps) of a track in one image. To simplify the illustration, we avoided to draw overlapping cells.

decreases with event duration and falls below 50% for events of 35 min and longer (Figure S4). This reflects the increasing probability of splitting and merging of rain cells for longer events. We observe a similar relation concerning the event size at the peak of the event (Figure S5). More than 50% of the events with a size of 5 km include splitting and/or merging, and this fraction increases for larger events. So larger events have longer durations and are more likely to be affected by splitting and merging.

Generally, the highest intensities are concentrated on a small-area fraction of a rain cell. Figure 2a shows a rain cell composite for the 1000 strongest precipitating events (at peak of the event) with dew points between 13°C and 20°C. A steep decrease of precipitation intensity with increasing distance from the center is clearly seen. A large fraction of the rain cell area has rather low precipitation intensities. The intensity profile (radial average) in Figure 2b further quantifies the sharp peak with a strong decline of precipitation intensity with distance to the center. Results for a subsample of events with lower humidity—between 5°C and 11°C dew point temperature—display a very similar dependency with distance to the center.

However, comparing the low-humidity sample with the high-humidity sample, we see much higher intensities throughout most of the rain cell in the latter. In addition to the increase in peak intensity, there is a coinciding increase in the area with high intensities. In other words, there are higher intensities within the same radius in the high-humidity sample without a clear sign of redistribution of intensities toward the center as suggested by *Wasko et al.* [2016]. The similarity between the distribution of intensity in the rain cell for low and high dew points motivates us to only look at the peak intensities of the event as relative changes in the peak intensity are representative for the overall intensity changes within the rain cell.

3.2. Precipitation Area, Intensity, and T_d

We first investigate the distribution of event size as a function of T_d at the peak of the event. Figure 3a shows that most of the events are rather small in size, more than 50% are typically below 4 km, and approximately

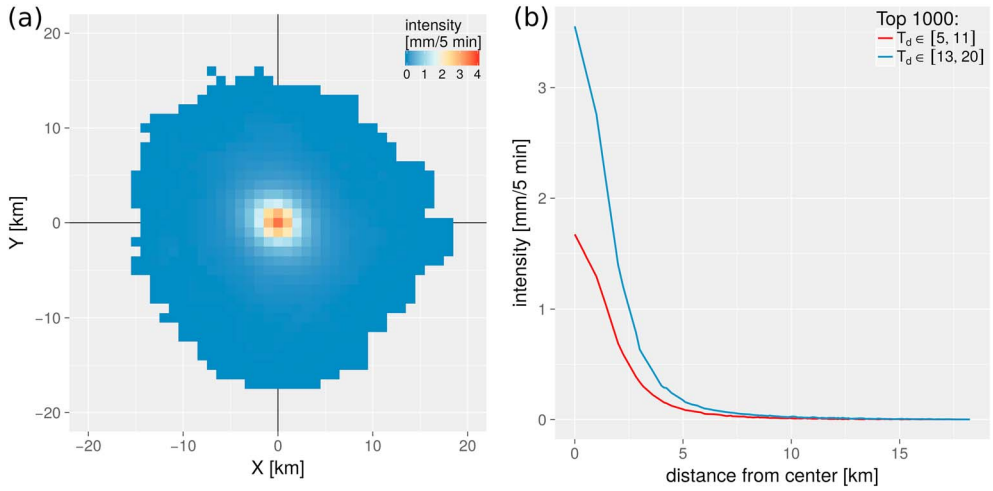

Figure 2. (a) Composite of the 1000 strongest precipitating events between 13°C and 20°C at the time of the event peak. The averaging was done centering cells on the intensity weighted center of mass ($x = 0$, $y = 0$). Grid points that are covered by less than 1% of the selected events are omitted. (b) Intensities steeply decrease with growing distance from the center. The blue curve shows a radially averaged profile for the composite in Figure 2a. The red curve represents a corresponding subsample for T_d between 5°C and 11°C.

10% exceed 7 km. The distribution of cell size depends on the dew point temperature. At lower humidity, below dew points of 10°C, we see a weak increase in event size for the highest percentile of the distribution. However, the size distribution changes much more clearly in the high-humidity range, at T_d above 15°C, where we see a progressive tendency toward bigger events.

Cell sizes conditioned on the rainfall intensity show a similar behavior. In Figure 3b we show the median cell size for a selection of events with different intensities. A rapid increase in cell size is visible for T_d beyond 15–16°C, but the increase in the low dew point range (below 10°C) is now almost nonexistent. In addition, it is found that cells with stronger intensity are larger. For instance, the selection of the 10% most intense events has a size of on average 6 km or more, almost double the average size of the lowest 50% intensity events. This correlation is by no means perfect. If there would be a perfect correlation of cell size and cell intensity (that is, a unique monotonic function exists to relate size to intensity and vice versa), then the 80th

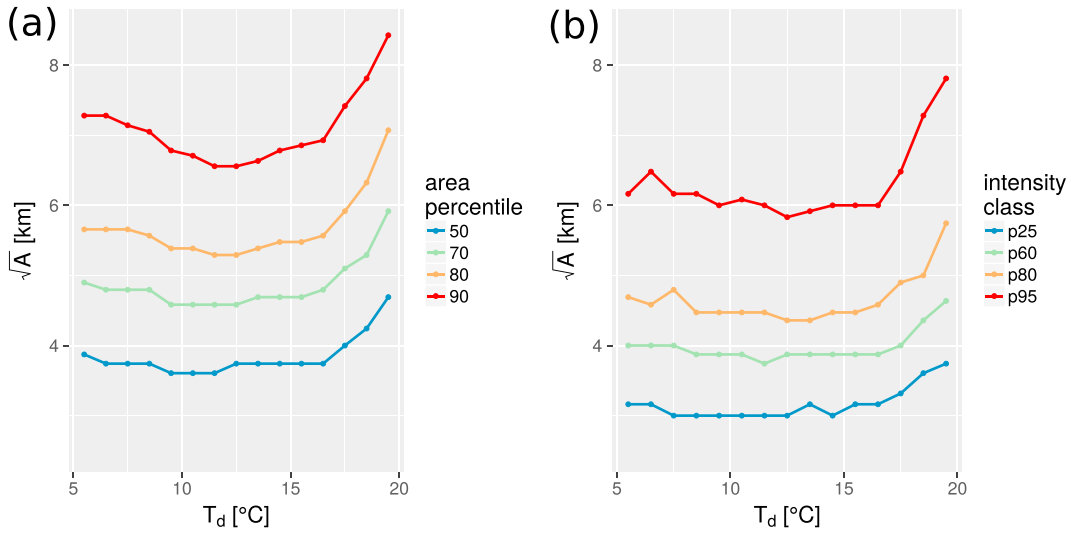

Figure 3. Cell size distribution (square root of the cell area at event peak) with respect to dew point temperature (derived using an equal bin width of 1°C). (a) Percentiles of the distribution of cell size and (b) cell size conditioned on the intensity, computed by plotting the median of the area of events with intensity below the 50th percentile (p25), between the 50th and 70th percentiles (p60), the 70th and 90th (p80), and above the 90th percentile (p95).

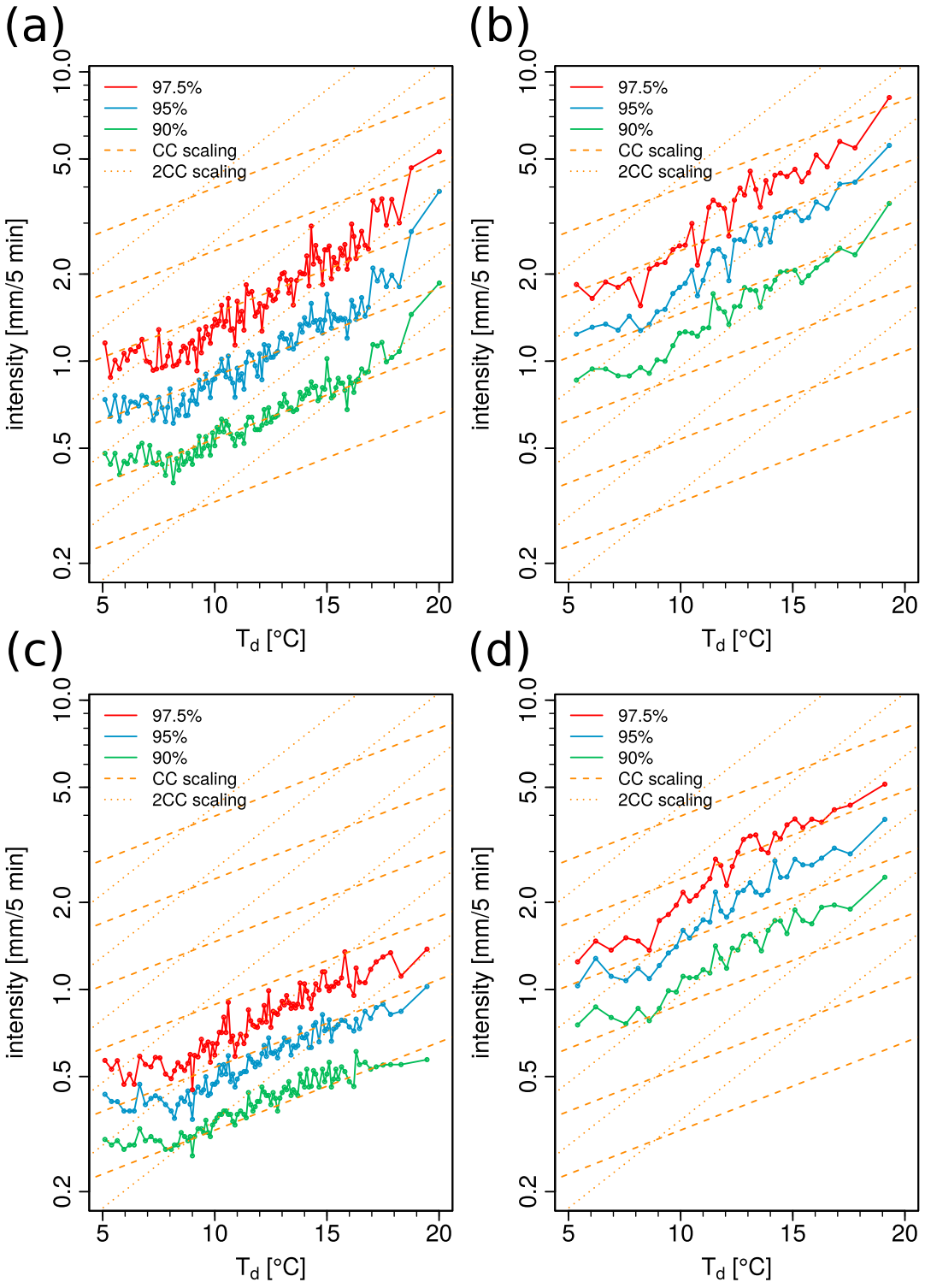

Figure 4. Extreme precipitation scaling with respect to dew point temperature. (a) The 90th, 95th, and 97.5th percentiles for all events. (b) The same as Figure 4a but for events with $\sqrt{A} > 5$ km. (c) The scaling for events with $\sqrt{A} \leq 5$ km only. (d) A subset of events with $\sqrt{A} \geq 5$ km and $\sqrt{A} \leq 9$ km. Dashed lines indicate CC scaling, and dotted lines indicate 2CC scaling.

percentile of the cell size (Figure 3a) should match exactly with the median of area of the events selected between the 70th and 90th intensity percentile (p80, in Figure 3b). So, event size and peak intensity are clearly positively correlated, but there is no unique relation between cell size and cell intensity.

3.3. Extreme Precipitation Scaling and Sensitivity to Event Size

Having found that on average bigger cells produce higher peak intensities, and that the event size distribution shifts toward bigger events beyond 15°C dew point temperature, we now focus on the role of events size to explain precipitation intensity scaling. Figure 4a shows the scaling of precipitation intensity with T_d for the 90th, 95th, and 97.5th percentiles (calculated per bin). In this case, the bins are constructed to contain approximately 1000 events.

Scaling rates are close to or exceed the CC relation for dew points above 8°C (Figure 4a). In general, scaling rates increase with dew point temperature and with increasing percentile. The scaling behavior of the 90th and 95th percentiles is rather similar; up to 15°C intensities follow an approximately constant rate of 7% $°C^{-1}$ (CC). For higher T_d we see an exceedance of the CC rate. The 97.5th percentile appears to have a slightly higher scaling rate on a wider T_d range.

The finding of a scaling rate close to the CC relation, or slightly above, up to dew points of 15°C, contradicts the results of previous studies which found a robust double CC scaling for (sub)hourly precipitation in the Netherlands across a much larger dew point range [*Lenderink and van Meijgaard*, 2008; *Loriaux et al.*, 2013]. However, we have seen that there is a clear link between intensity and event size (see Figure 3b). Therefore, we split the event catalog using a size threshold of 5 km and repeat the binning procedure. This 5 km threshold divides the data approximately into 70% small-area events and 30% large-area events (see Figure 3a). The large-area events not only have higher intensities than the small-area events but also higher scaling rates (Figures 4b and 4c). Whereas for the small-area events precipitation extremes scale with rates close to CC over the whole dew point temperature range, large-area events clearly exceed the CC scaling rate.

Using a higher event size threshold, for instance 7 km (Figure S6), confirms the increased scaling rate for bigger events. The diagnosis of a scaling rate close to the CC relation for smaller event sizes tends to be robust even if we omit very small events (Figure S7). Specifically looking at solitary tracks, which are dominant below the applied area thresholds, yields a scaling close to the CC relation, but with a slightly higher rate for the most extreme events (Figure S8). In contrast to that, splitting and merging tracks have higher extremes that increase stronger with dew point temperature (Figure S9).

Considering that larger events have higher scaling rates, it is natural to question the role of the increase in event size beyond 15–16°C dew point temperature. In order to investigate this we limited event size to a minimum of 5 km and a maximum of 9 km (Figure 4d). While in the intermediate dew point temperature regime up to 15°C, scaling rates still exceed the CC rate (close to 2CC), at higher dew point temperatures the scaling rate falls back to the CC rate. This fallback to CC rate also clearly shows up using a larger dew point bin size (compare Figures S10a and S10b). Thus, the results are robust and independent of the chosen bin size. We conclude that the inclusion of the biggest events is needed in order to maintain an enhanced scaling rate at the highest dew point temperatures. So a super CC scaling at the highest dew point temperature range can only be sustained if there is an accompanying increase in event size.

To quantify the dependence of the intensity scaling on event size further, we calculate a scaling coefficient (fractional rate of change of precipitation intensity per degree T_d) $\alpha = \log(r)/(\bar{T}_{d,1} - \bar{T}_{d,2})$, where $r = P_{i,T_{d,1}} / P_{i,T_{d,2}}$ [*Moseley et al.*, 2013]. For that, we take events from two T_d ranges: 5°C to 11°C (2) and 13°C to 20°C (1). $\bar{T}_d$ is the corresponding group mean of dew point temperature and P_{i,T_d} the respective ith intensity percentile with $i \in \{90, 95\}$.

Figure 5 summarizes the results of this analysis. Including all events in the two T_d ranges, α varies between 7.8% $°C^{-1}$ and 9.9% $°C^{-1}$. For the area-constrained analysis with $\sqrt{A} \leq 5$ km and $\sqrt{A} \leq 6$ km we obtain smaller scaling rates between 6.7% $°C^{-1}$ and 9% $°C^{-1}$. Setting a minimum area threshold, scaling rates are mostly beyond 11% $°C^{-1}$. For both percentiles α steadily increases with respect to the area threshold and reaches values around 13% $°C^{-1}$ for $\sqrt{A} \geq 8$ km. Note that we excluded the 97.5th percentile as there are successively decreasing sample sizes at higher area thresholds. A reliable estimation of this quantile cannot be guaranteed under this circumstance. So we clearly see a scaling close the CC relation if the event size is constrained to 5–6 km, whereas bigger events scale close to 11–13% per degree.

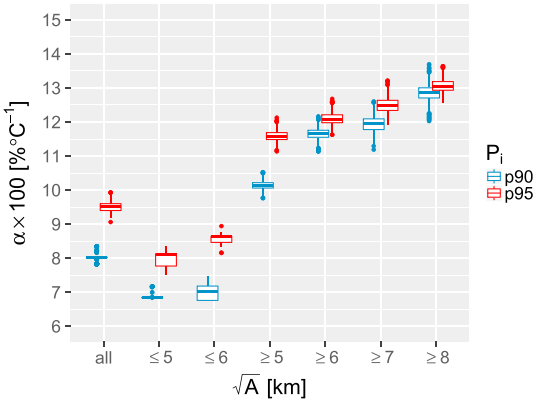

Figure 5. The scaling parameter α for different percentiles and area-constrained subsamples. Uncertainties are estimated repeating the calculation 1000 times while randomly dropping 10% of the events.

4. Conclusions and Discussion

In this paper we analyzed the characteristics of showers at the time of their peak intensity using a tracking of rain cells in 9 years of rain radar data of summertime conditions over the Netherlands. Using dew point temperature, we investigated how event size (defined as the square root of cell area at the time of peak intensity) and intensity depend on near-surface moisture as measured by the 2 m dew point temperature. In general, the results show that event peak intensity and cell area are clearly related; in a statistical average stronger events are larger events. Additionally, event sizes increase remarkably at dew point temperatures above 15°C.

The scaling of peak intensities with dew point temperature is strongly tied to the rain cell area and only larger events can display the super CC scaling. Events below an area threshold of 5–6 km display a dependency of peak intensities following a rate close to the CC relation, predicting 6–7% $°C^{-1}$. Conversely, events which exceed the minimum event size show a scaling of peak intensities of approximately 11% to 13% per degree.

Beyond a dew point temperature of 15°C, super CC scaling can only be sustained with a corresponding rapid increase in rain cell size. This has been found by omitting the largest events from the sample, which causes the scaling rate to fall back to CC rate above 15°C dew point. It is interesting to note that at approximately the same dew point temperature range strong feedbacks caused by latent heat come into play [*Lenderink et al.*, 2017]. This feedback leads (i) to strongly buoyant cloud updrafts and very deep convective clouds and (ii) enhanced large-scale moisture convergence due to enhanced large-scale vertical velocities. Finally, we mention a possible link to the critical behavior as seen in tropical convection, where beyond a critical value of integrated water vapor content a steep increase in cloud size and intensity is observed [*Neelin et al.*, 2009].

The finding that intensities increase rather uniformly over the rain cell area with dew point temperature, and the cell size increase, indicates that the shower sources moisture from a larger area. A super CC scaling of rainfall rates within the cell must be supported by a moisture transport also in excess of the CC relation, and assuming the same source area the transport would increase only at the CC rate [*Westra et al.*, 2014]. We note, however, that the whole life cycle of convective cells/events must be considered to be able to give a more definite answer. Nevertheless, we do not find any evidence of a redistribution of moisture toward the center at the cost of the outer region of the rainfall area as found by *Wasko et al.* [2016].

In summary, our results reveal that the cloud cell size plays a crucial role in the mechanism behind the super CC scaling of convective clouds. Larger events are more likely a product of merging and splitting of rain cells, and this probability further increases at dew point temperatures above 15°C where event sizes increase rather steeply. This suggests that the organization of convective showers into larger clusters is of importance in the context of super CC scaling, in accordance with a recent modeling study [*Moseley et al.*, 2016]. In contrast, super CC behavior was not obtained in simulations of rather weakly organized convection [*Loriaux et al.*, 2017] and also not found for solitary tracks [*Moseley et al.*, 2016]. Therefore, we think that understanding the mesoscale atmospheric and cloud dynamics is crucial to be able to better predict and understand future changes in convective storms: their intensity, size, heterogeneity, and level of aggregation [e.g., *Guinard et al.*, 2015; *Pendergrass et al.*, 2016; *Westra et al.*, 2014].

Acknowledgments
The authors are grateful for the funding from the Netherlands Organisation for Scientific Research (NWO), project Space2rain (869.15.002). Lenderink acknowledges financial support from the project INTENSE, which is supported by the European Research Council (grant ERC-2013-CoG, project 617329). We also acknowledge Aart Overeem for his support during the preprocessing of the rain radar data set. A data set with the event catalog is available at http://doi.org/10.4121/uuid:a00ab095-fb31-44e8-a77c-587063a5839e.

References

Allen, M. R., and W. J. Ingram (2002), Constraints on future changes in climate and the hydrologic cycle, *Nature*, *419*(6903), 224–232, doi:10.1038/nature01092.

Guinard, K., A. Mailhot, and D. Caya (2015), Projected changes in characteristics of precipitation spatial structures over North America, *Int. J. Climatol.*, *35*(4), 596–612, doi:10.1002/joc.4006.

Haerter, J. O., and P. Berg (2009), Unexpected rise in extreme precipitation caused by a shift in rain type?, *Nat. Geosci.*, *2*(6), 372–373, doi:10.1038/ngeo523.

Kharin, V. V., F. W. Zwiers, X. Zhang, and M. Wehner (2013), Changes in temperature and precipitation extremes in the CMIP5 ensemble, *Clim. Change*, *119*(2), 345–357, doi:10.1007/s10584-013-0705-8.

Lenderink, G., and E. van Meijgaard (2008), Increase in hourly precipitation extremes beyond expectations from temperature changes, *Nat. Geosci.*, *1*(8), 511–514, doi:10.1038/ngeo262.

Lenderink, G., and E. van Meijgaard (2010), Linking increases in hourly precipitation extremes to atmospheric temperature and moisture changes, *Environ. Res. Lett.*, *5*(2), 025208, doi:10.1088/1748-9326/5/2/025208.

Lenderink, G., H. Mok, T. Lee, and G. Van Oldenborgh (2011), Scaling and trends of hourly precipitation extremes in two different climate zones—Hong Kong and the Netherlands, *Hydrol. Earth Syst. Sci.*, *15*(9), 3033–3041, doi:10.5194/hessd-8-4701-2011.

Lenderink, G., R. Barbero, J. M. Loriaux, and H. J. Fowler (2017), Super Clausius-Clapeyron scaling of extreme hourly convective precipitation and its relation to large-scale atmospheric conditions, *J. Clim.*, *30*(15), 6037–6052, doi:10.1175/JCLI-D-16-0808.1.

Loriaux, J. M., G. Lenderink, S. R. D. Roode, and A. P. Siebesma (2013), Understanding convective extreme precipitation scaling using observations and an entraining plume model, *J. Atmos. Sci.*, *70*(11), 3641–3655, doi:10.1175/JAS-D-12-0317.1.

Loriaux, J. M., G. Lenderink, and A. P. Siebesma (2017), Large-scale controls on extreme precipitation, *J. Clim.*, *30*(3), 955–968, doi:10.1175/JCLI-D-16-0381.1.

Mishra, V., J. M. Wallace, and D. P. Lettenmaier (2012), Relationship between hourly extreme precipitation and local air temperature in the United States, *Geophys. Res. Lett.*, *39*, L16403, doi:10.1029/2012GL052790.

Molnar, P., S. Fatichi, L. Gaál, J. Szolgay, and P. Burlando (2015), Storm type effects on super Clausius-Clapeyron scaling of intense rainstorm properties with air temperature, *Hydrol. Earth Syst. Sci.*, *19*(4), 1753–1766, doi:10.5194/hess-19-1753-2015.

Moseley, C., P. Berg, and J. O. Haerter (2013), Probing the precipitation life cycle by iterative rain cell tracking, *J. Geophys. Res. Atmos.*, *118*, 13,361–13,370, doi:10.1002/2013JD020868.

Moseley, C., C. Hohenegger, P. Berg, and J. O. Haerter (2016), Intensification of convective extremes driven by cloud-cloud interaction, *Nat. Geosci.*, *9*(10), 748–752, doi:10.1038/ngeo2789.

Neelin, J. D., O. Peters, and K. Hales (2009), The transition to strong convection, *J. Atmos. Sci.*, *66*(8), 2367–2384, doi:10.1175/2009JAS2962.1.

Overeem, A., I. Holleman, and A. Buishand (2009a), Derivation of a 10-year radar-based climatology of rainfall, *J. Appl. Meteorol. Climatol.*, *48*(7), 1448–1463, doi:10.1175/2009JAMC1954.1.

Overeem, A., T. A. Buishand, and I. Holleman (2009b), Extreme rainfall analysis and estimation of depth-duration-frequency curves using weather radar, *Water Resour. Res.*, *45*, W10424, doi:10.1029/2009WR007869.

Pall, P., M. R. Allen, and D. A. Stone (2007), Testing the Clausius–Clapeyron constraint on changes in extreme precipitation under CO_2 warming, *Clim. Dyn.*, *28*(4), 351–363, doi:10.1007/s00382-006-0180-2.

Pendergrass, A. G., K. A. Reed, and B. Medeiros (2016), The link between extreme precipitation and convective organization in a warming climate: Global radiative-convective equilibrium simulations, *Geophys. Res. Lett.*, *43*, 11,445–11,452, doi:10.1002/2016GL071285.

Tebaldi, C., K. Hayhoe, J. M. Arblaster, and G. A. Meehl (2006), Going to the extremes, *Clim. Change*, *79*(3), 185–211, doi:10.1007/s10584-006-9051-4.

Trenberth, K. E., A. Dai, R. M. Rasmussen, and D. B. Parsons (2003), The changing character of precipitation, *Bull. Am. Meteorol. Soc.*, *84*(9), 1205–1217, doi:10.1175/BAMS-84-9-1205.

Wasko, C., and A. Sharma (2015), Steeper temporal distribution of rain intensity at higher temperatures within Australian storms, *Nat. Geosci.*, *8*(7), 527–529.

Wasko, C., A. Sharma, and F. Johnson (2015), Does storm duration modulate the extreme precipitation-temperature scaling relationship?, *Geophys. Res. Lett.*, *42*, 8783–8790, doi:10.1002/2015GL066274.

Wasko, C., A. Sharma, and S. Westra (2016), Reduced spatial extent of extreme storms at higher temperatures, *Geophys. Res. Lett.*, *43*, 4026–4032, doi:10.1002/2016GL068509.

Westra, S., H. J. Fowler, J. P. Evans, L. V. Alexander, P. Berg, F. Johnson, E. J. Kendon, G. Lenderink, and N. M. Roberts (2014), Future changes to the intensity and frequency of short-duration extreme rainfall, *Rev. Geophys.*, *52*, 522–555, doi:10.1002/2014RG000464.